International Journal of Advances in Engineering and Management (IJAEM)
Volume 4, Issue 4 Apr 2022, pp: 706-716 www.ijaem.net ISSN: 2395-5252

Structures, Electronic, and Transport Properties of M_2PbC (M=Zr, V)

S. T. Ahams[a,b]*, A. Shaari[a], N. F. Abdul Pattah[a], M. Buba[a.c]

[a]*Department of Physics, Universiti Teknologi Malaysia. Johor Bahru*
[b]*Department of Pure and Applied Physics, Adamawa State University, Mubi, Nigeria.*
[c] *Department of Science Laboratory Technology, Federal Polytechnic, Mubi, Nigeria*

Submitted: 05-04-2022 Revised: 16-04-2022 Accepted: 19-04-2022

ABSTRACT: This study investigates the electronic, and transport properties of M2PbC (M=Zr, V) MAX phases based on density functional theory density functional perturbation theory, and Boltzmann transport theory, respectively. The electronic and density of states show the V, and Zr containing MAX phases have metallic characteristics. The energy bands at the Fermi level (EF) and elsewhere within its vicinity, are mainly contributed by the V 3d, Zr 4d, and the Pb 6p states. A V_ Pb, Zr _ Pb, hybridizations occur just below the EF and stretch through to the conduction band, the effects of which are more strongly felt than the Zr-C, V-C bonds. The phonon contribution to thermal conductivity at finite temperature is low compared to electron contribution. From the calculated transport coefficients, a complete replacement of Zr with V expands the thermoelectric figure of merit from 0.026 for Zr2PbC to 0.13 for V2PbC, respectively.

KEYWORDS: MAX phase, metallic, hybridization, thermal conductivity, thermoelectric figure of merit

I. INTRODUCTION

In the universal quest to fight global warming, clean energy bases are eminent [1], [2]. Thermoelectricity directly converts waste heat or temperature gradient to an electrical potential difference using the Seebeck effect[3]–[5]. The birth of the Seebeck effect in the early 1800s has many applications in today's engineering requirements, however, a lot of challenges thwart so many efforts of maximizing the efficiency of thermoelectric devices[6]–[9]. Statistical results show that over 60% of energy is laid waste globally, mostly in the form of waste heat[10]. Research interest in thermoelectricity (TE) has attracted growing attention recently [4]. An efficient TE device is determined by the (ZT) [11] expressed in equation (1).

$$ZT = \frac{S^2\sigma}{k_{el} + k_{lat.}}T \qquad (1)$$

where ZT is a dimensionless quantity, S represents the Seebeck coefficient, σ and k_e the electrical and thermal conductivities, and $S^2\sigma$ the power factor, respectively. To attain the best performance, ZT must be enhanced by maximizing the power factor $S^2\sigma$ which minimizes the k_e.The $S^2\sigma$ is a key factor in understanding the thermoelectric properties of a material [12]. However, these three parameters ($S, \sigma,$ and $k_{el}, k_{lat.}$) depend on each other. Therefore, the challenge to establish support for a TE material with high ZT is to simultaneously achieve a high Seebeck coefficient, high electrical conductivity, low electronic thermal conductivity, and low phonon thermal conductivity[13].

In recent years, MAX phase materials have propelled the focus of researchers for their enormous potential and TE may just be one of the novels upcoming. Magnuson et al. (2011) have studied the Seebeck factor in Ti_3SiC_2 single-crystal thin films and have traced the source to anisotropies in element-specific electronic states. They found that the bulk form of Ti_3SiC_2 has a Seebeck factor of almost zero over a large temperature spectrum. On the contrary, however, the in-plane (basal ab) Seebeck coefficient of Ti_3SiC_2, calculated on single-crystal films, has a substantially positive Seebeck coefficient of 4 to 6 μV/K[14]. Series of ab-initio computations were conducted to investigate the transportation in monolayers and multilayers of the functionalized M_2C (M = Sc, Ti, V, Zr, Nb, Mo, Hf, Ta), and M_2N (M = Ti, Zr, Hf) using F, O, and OH[15]. Though relaxation time (τ) is an undefined factor in their

International Journal of Advances in Engineering and Management (IJAEM)
Volume 4, Issue 4 Apr 2022, pp: 706-716 www.ijaem.net ISSN: 2395-5252

evaluations, a comparison of the transport coefficients of MXenes is still justifiable. The simple reason is that the MXenes here have structures analogous to MAX phase structures as they were initially etched from a family of nanolaminates [16].

MAX phases have a universal stoichiometry of $M_{n+1}AX_n$[17]–[19], wheren $= 1, 2,$ or 3 and represents an integer, M is a transition metal, A is found in group A element which is largely found in group III-A, IVA, X stands for C/N [20]. The group crystalizes into a hexagonal shape of space group P63/mmc[21]–[24]. This family of compounds has been widely explored recently due to their exceptional and dual characteristics as a metal and as a ceramic[17], [25]–[27]. Akin to metals, they serve as excellent thermal and electric electrodes having a remarkable thermal shock and damage tolerance [28]–[30]. Nanolaminates are known to show endurance to corrosion and oxidation [31], [32]. Mostly elastic and yet extremely easy to machine [33], [34], which are some of the salient physical characteristics that make the MAX phases suitable for many potential applications where resistance to ultra-high-temperature, radiation damage tolerance, self-lubrication, and so on are some of the key factors to look for[35]–[37]. Reliant on the integer, n, MAX phases are grouped into a class of 211 (n = 1), 312 (n = 2), 413(n = 3) and 514(n = 4) phases and so on[38].

High-performance ZT is one recent area of research interest in condensed matter due to its practical applications as a clean power generation material from waste-heat supplies like power plants and automobile machines[39]. Because of the presence of both electronic and thermal transport processes, as well as non-equilibrium transport processes, the properties required to understand electrical transport and thermoelectric properties of MAX phases are difficult to calculate from the first principles[40]. Whence, MAX phases have been studied as precursors for MXenes of family formula ($M_{n+1}X_n$), a 2D nanosheet with properties analogous to that of graphene currently only synthesizable through a selective chemical etching of, largely the Al-based MAX phases[41]. In a related review on the structural, elastic, thermodynamic, and optical properties of Zr_2PbC, the structure has been reported to be unstable at normal pressure and temperature[42]. As there are just but few pieces of works of literature that have either directly or otherwise studied the ZT of Zr_2PbC and V_2PbC, this research paper aims at providing a systematic cross-examination of their electronic and thermoelectric properties respectively, for the first time.

II. COMPUTATIONAL FRAMEWORK

The ternaries Zr_2PbC and V_2PbC MAX phases have been investigated based on first principles using density functional theory [43][44]as implemented in Quantum Espresso (QE)[45], [46]simulation package and the Boltzmann transport theory[47], [48]. The generalized gradient approximation (GGA-PBE)[49] exchange energy was used. Throughout this study, ultrasoft pseudopotentials (UPP) have been employed and an energy cut-off of 800 Ry was applied to limit the number of components in the plane wave expansion. A Gaussian smearing technique has been used to a smearing width of 2.0 $\times 10^{-2}$ Ry. A 16 × 16 × 6 k-points mesh has been produced utilizing the Monkhorst-Pack program for the Brillouin zone integration, [50] to generate a uniform k-points grid along with the a, b, c -axes in reciprocal space. The BFGS (Broyden–Fletcher–Goldfarb-Shenno) method has been used to optimize the lattice parameters and was fully optimized after relaxing the atomic positions through several volumes to a threshold of approximately about 1.0×10^{-8} Ry[50]. Transport properties were evaluated using Boltzmann transport theory as implemented in the BoltzTraP2 simulation code [47], [48], while the phonon contribution to thermal conductivity was calculated using the D3Q simulation pack as implemented in quantum espresso 6.7 [46]Within this approximation, the Seebeck coefficient becomes τ-independent without any other adjustable parameter, but the electrical conductivities and the power factors are obtained for τ. BoltzTraP2 computes the transport coefficients centered on the rigid-band approximation (RBA), which accepts that changing the temperature, or alloying (doping) a system, does not change the band structure. In the rigid band approximation (RBA) the density of the materials of states $(n(\varepsilon))$ can be calculated by applying Equation (2);

$$n(\varepsilon) = \int \sum_{b} \delta(\varepsilon - \varepsilon_{b,k}) \frac{d\mathbf{k}}{8\pi^3} \qquad (2)$$

where the b operates over the bands. A linearized edition of the BTE has been employed under the RTA, where the energy and temperature-dependent transport distribution function, $\sigma(\varepsilon, T)$given by Equation (3) is applied for calculating the moments, Equation (4) of the generalized transport coefficients, $\mathcal{L}^{(\alpha)}(\mu; T)$[48], [51]

International Journal of Advances in Engineering and Management (IJAEM)
Volume 4, Issue 4 Apr 2022, pp: 706-716 www.ijaem.net ISSN: 2395-5252

$$\sigma(\varepsilon, T) = \int \sum_{b} \mathbf{v}_{b,k} \times \mathbf{v}_{b,k} \tau_{b,k} \delta(\varepsilon - \varepsilon_{b,k}) \frac{d\mathbf{k}}{8\pi^3} \quad (3)$$

where $\mathbf{v}_{b,k}$ represents the group velocities, $\tau_{b,k}$relaxation time approximation (RTA)

$$\mathcal{L}^{(\alpha)}(\mu; T) = q^2 \int \sigma(\varepsilon, T)(\varepsilon - \mu)^{\alpha} \left(-\frac{\partial f^{(0)}(\varepsilon; \mu, T)}{\partial \varepsilon}\right) d\varepsilon \quad (4)$$

where $\mathcal{L}$ denotes the generalized transport coefficients, and $f^{(0)}$represents the Fermi distribution function. The Seebeck coefficient (S), electrical, and thermal conductivities (σ_τ, k_{el}) due to charge carrier contribution at and around the Fermi can thus be calculated by applying Equations (5) to (7), respectively.

$$\sigma_\tau = \mathcal{L}^{(0)} \quad (5)$$

$$S = \frac{1}{qT} \frac{\mathcal{L}^{(1)}}{\mathcal{L}^{(0)}} \quad (6)$$

$$k_{el} = \frac{1}{q^2 T} \left[\frac{\left(\mathcal{L}^{(1)}\right)^2}{\mathcal{L}^{(0)}} - \mathcal{L}^{(2)} \right] \quad (7)$$

Table 1. Once self-consistency, or the minimum, has been reached, the total energy [52]of the system is calculated.

3.2. Electronic properties

All the electronic and bonding physical characteristics were investigated to ascertain the electrical behaviours of Zr_2PbC and V_2PbC. The calculated energy bands are depicted in Figures 2 (a), and (b), respectively. With practically zero bandgaps at the Fermi level (represented with the horizontal black dash line, there is a lot of overlapping of the valence and conduction bands

$$E_0 = \sum_{i} f_i \varepsilon_i - E_H[n(r)] + E_{XC}[n(r)] - \int n(r) V_{XC}[n(r)]\, dr + E_{ion-ion} \quad (8)$$

III. RESULTS AND DISCUSSIONS.

3.1. Structural properties.

The 211 layered ternaries, Zr_2PbC, and V_2PbC crystallize into the hexagonal structure of space group P63/mmc like any other MAX compound. Their unit cell contains two formula units of eight atoms each. The atomic coordinates of atoms which are located thus: Zr/V (0.33, 0.67, z), Pb (0.67, 0.33, 0.25) and C (0, 0, 0), respectively. Figure 1 shows the unit cell structures of Zr_2PbC, and V_2PbC, respectively. The equilibrium crystal structure of these compounds has been attained by minimizing the total energy[52] Equation (8).

where E_0 the total ground state total energy, $\varepsilon_i$is one-electron contributionE_H is the Hartree contribution, E_{XC} is the exchange contribution, and the fourth and fifth terms are the ewald contributions.

The calculated results for V_2PbC have been compared with literature data of the parent material Zr_2PbC. A Series of geometry optimizations were conducted on the completely relaxed coordinates of V_2PbC and Zr_2PbC to obtain the structural parameters from the optimized volume. During such calculations, fixed unit cell volume has been considered, and several readings of separate axial ratios of c/a are obtained to evaluate the total and minimum energy E_{min} as recorded in

inherent to the two studied nanolaminate which is akin to their metallic behaviours. With these flash characteristics, Zr_2PbC, and V_2PbC are projected to exhibit electrical, and thermal conductivities just like any other MAX phase. There is an important feature foreseen of the band structure which is a solid anisotropy with less energy dispersion on the c-axis observed from a reduced dispersion down the short Γ_A, L_M, and K_H paths as displayed in Figure 2 (a) and (b), respectively.

International Journal of Advances in Engineering and Management (IJAEM)
Volume 4, Issue 4 Apr 2022, pp: 706-716 www.ijaem.net ISSN: 2395-5252

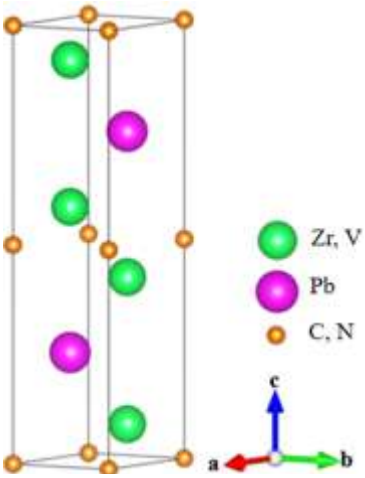

Figure 1. Crystal structure of M_2PbC

To understand the atomic bonding behaviours in the ternary layered materials, the total, and partial densities of states (TDOS, and PDOS) have been computed and compared as presented in Figures(a) and (b), respectively. This spans across a range of -12 to +5 electronvolts, while C -2p and Pb -6p states demonstrate satisfactory impact in the valence band within the energy -5 eV to -1 eV and -7 eV to -1 eV, respectively in the two cases for Zr_2PbC, and V_2PbC. The peaks in the TDOS for V_2PbC are manifest from the enormous contributions of the V -3d, Pb-6p, and C -2p, states as depicted in Figure 3(b). The TDOS peak at the E_F is a result of the practically visible contributions from V -3d and Pb -6p, while C -2p and Pb -6s are the builders of the TDOS in the range of -7 eV to -2 eV. On the other hand, the V -3d, Pb -6p C -2p, are the results we see manifesting in the TDOS in the conduction band. The calculated TDOS for each of the ternaries at the E_F is 1.84 and 4.62 states/eV, respectively. The results imply that V_2PbC conducts more readily than Zr_2PbC. Generally, the nanolaminates have remarkably solid M-X bonds and moderately weak M-A bonds. Generally, the Zr/V d-orbitals and Pb p-orbital, respectively share major factors responsible for the conduction properties of the studied MAX compounds.

3.3. Transport properties

The Seebeck coefficient (S), power factor ($S^2\sigma_\tau$), electrical conductivity(σ/τ), and electronic thermal conductivity (k_{el}) of Zr_2PbC and V_2PbC has been calculated from the semiclassical Boltzmann transport theory. The calculated electronic structure data, E(n,k), Equations (3) and (4) have been used in calculating the transport coefficients of k_{el}, σ, and S using Equations (5), (6), and (7), respectively[51] while the phonon contribution ($k_{lat.}$,) which is very insignificant is calculated using D3Q and is compared to the electronic contribution.

The figure of merit ZT has been evaluated using Equation (1). An energy range of E-μ = ±0.15 Ry has been used to evaluate the integrals in Equations (2) to (4). The temperature range of interest for all the reported results is 200 K to 800 K with a step size of 200. Plots and results for the calculated TPs for Zr_2PbC and V_2PbC are displayed in Table 2, Figures 5 (a) to (d), and Figures 6(a) to (d), respectively.

The magnitude of S for bulk Zr_2PbC and V_2PbC MAX phases varies directly to the temperature which is clearly shown in Table 2 and Figure 5 (a) and Figure 6 (a), respectively. The Seebeck has increased significantly from 25.5 μVK^{-1} for Zr_2PbC at E-μ =0.075 Ry to 64.4 for V_2PbC at E-μ = -0.125 Ry, respectively. Which is a good indication that the nanolaminate V_2PbC has a more promising stand compared to Zr_2PbC as future thermoelectric material.

The calculated power factor, electrical and thermal conductivities, and figure of merit show that the substitution of Zr with V rises the electrical and thermal conductivities as well as increases the ZT as recorded in Table 2 and depicted in Figure 8 respectively. Hence, the calculated results at temperature 800 K, shows Zr_2PbC has a lower value of S, $S^2\sigma_\tau$, σ_τ, k_{el}, and ZT, respectively compared to V_2PbC which is depicted in Table 2.and Figure 5, and Figure 7. The difference in the electrical conductivity agrees well with the simulated density of state (TDOS).

The calculated ZT Figure 8 shows that Zr_2PbC and V_2PbC can be tuned through substitution or alloying on the M site with an

International Journal of Advances in Engineering and Management (IJAEM)
Volume 4, Issue 4 Apr 2022, pp: 706-716 www.ijaem.net ISSN: 2395-5252

appropriate transition metal Figures8 (a) and (b). The calculated band structures, TDOS, and PDOS completely validate the transport of our results.

As there are no literature results on the new ordered V_2PbC MAX phase available, the results of the parent material Zr_2PbC have been used for comparison where necessary and available. The contribution to thermal conductivity is greater due to the substitution of Zr with V on the M-site in bulk V_2PbC than in the bulk Zr_2PbC. For the given operating temperature range, the calculated ZT for V_2PbC is 0.133, far superior to that of the parent Zr_2PbC (ZT = 0.026) for the same temperature results which are shown in Figure 8 (b) and (a) plots and recorded in Table 2, respectively.

Table 1Equilibrium dimensional constants a, and c, the ratio c/a, volume V,and minimum energy E_{min}.

MAX Phase	A (Å)	c (Å)	c/a	V (Å^3)	E_{min} (Ry)	Reference
Zr_2PbC	3.402	14.93	4.39	150.5	-693.73	This work
	3.38	14.66	4.34			[53]
	3.42	14.95	4.37			[36]
V_2PbC	3.153	11.52	3.65	116.7	-877.96	This work

Table 2. Calculated Seebeck (S), power factor ($S^2\sigma_\tau$), electrical and thermal conductivities (σ, andk_e), and figure of merit (ZT) for Zr_2PbC and V_2PbC as a function of energy.

Comp.	S (μV/K)	$S^2\sigma_\tau$ (10^9 W/K·m)	σ_τ ($10^{18}\Omega\cdot m)^{-1}$	k_{el} (10^{15} W/m·K)	ZT
Zr_2PbC	25.50	2.00	6.20	11.81	0.026
V_2PbC	64.40	6.20	4.00	7.30	0.133

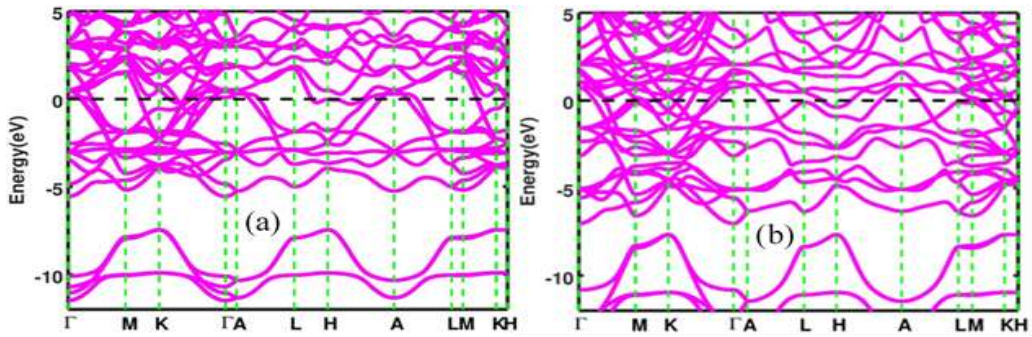

Figure 2. Calculated energy bands of (a) Zr_2PbC, and (b) V_2PbC

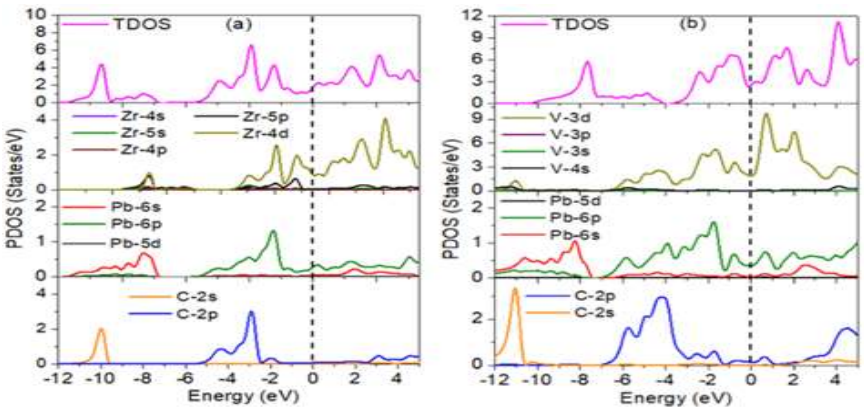

Figure 3. Total, and partial density of states of (a) Zr_2PbC, and (b) V_2PbC

International Journal of Advances in Engineering and Management (IJAEM)
Volume 4, Issue 4 Apr 2022, pp: 706-716 www.ijaem.net ISSN: 2395-5252

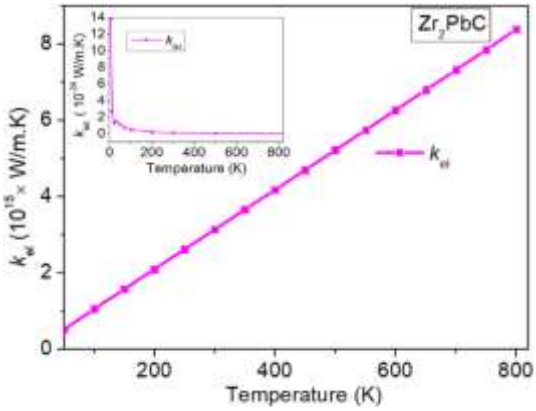

Figure 4. Electronic thermal conductivity with an inset of lattice contribution for Zr_2PbC

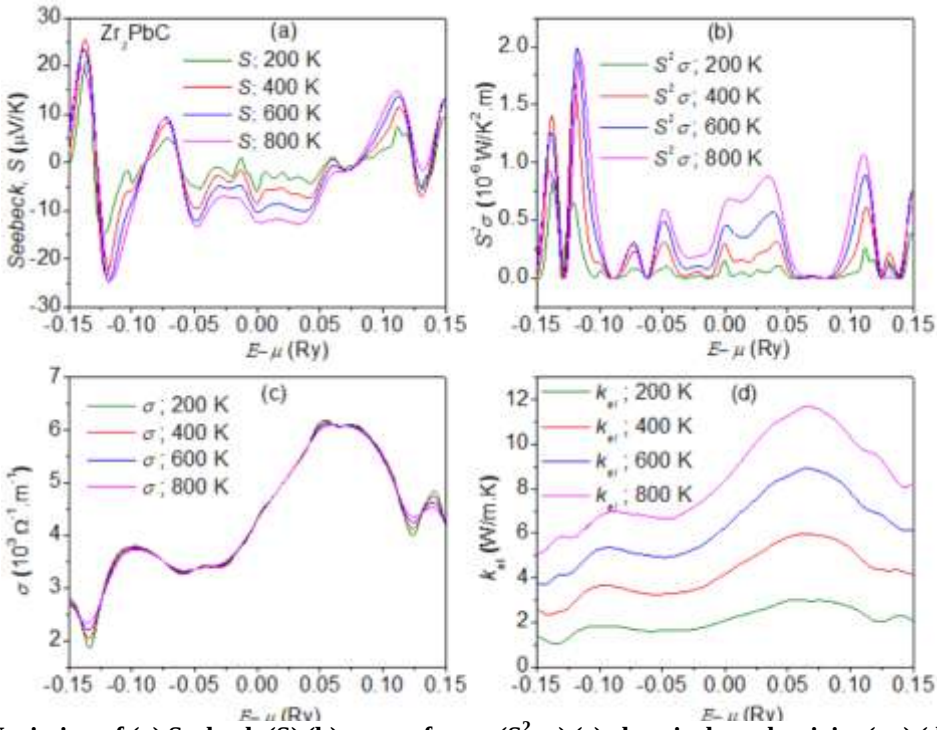

Figure 5. Variation of (a) Seebeck (S) (b) power factor ($S^2\sigma_\tau$) (c) electrical conductivity (σ_τ) (d) thermal conductivity (k_{el}) of Zr_2PbC

International Journal of Advances in Engineering and Management (IJAEM)
Volume 4, Issue 4 Apr 2022, pp: 706-716 www.ijaem.net ISSN: 2395-5252

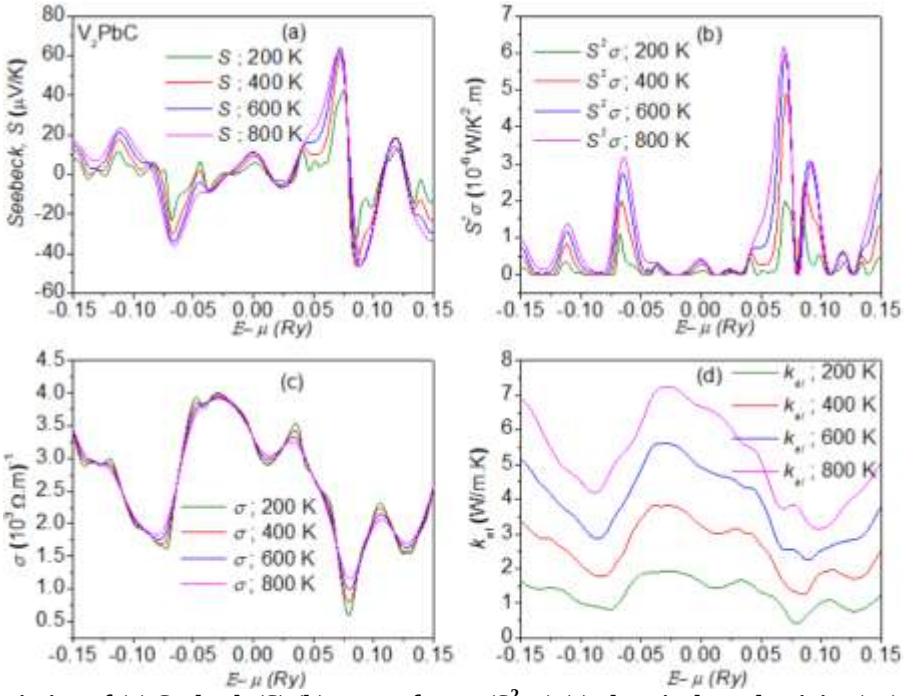

Figure 6. Variation of (a) Seebeck (S) (b) power factor ($S^2\sigma_\tau$) (c) electrical conductivity (σ_τ) (d) thermal conductivity (k_{el}) of V_2PbC

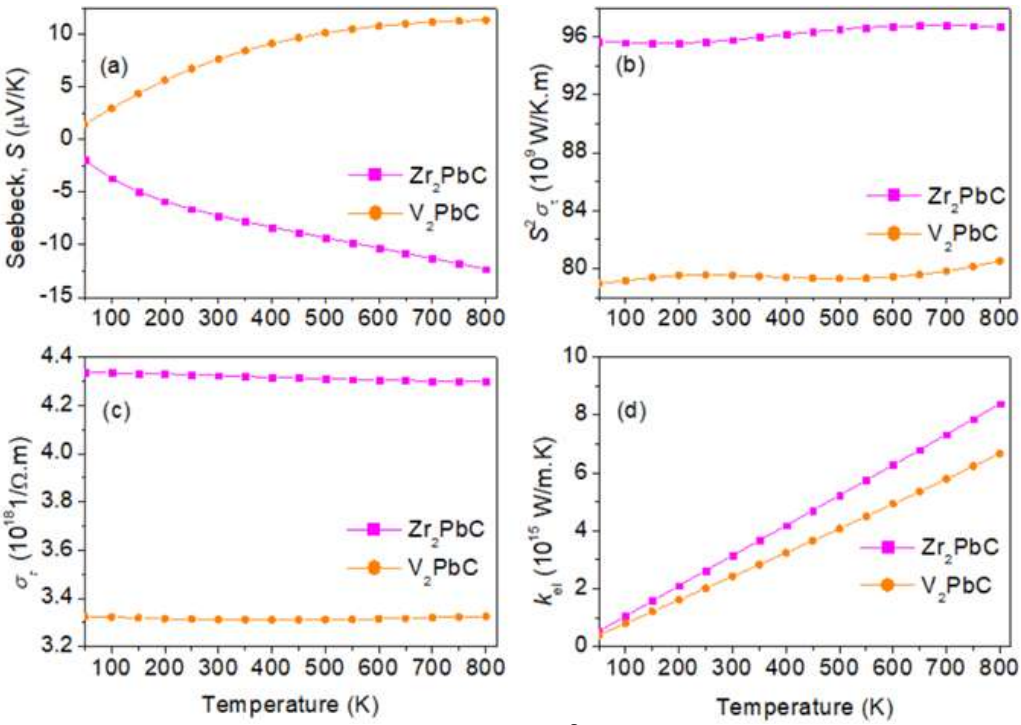

Figure 7. Variation of (a) Seebeck (S) (b) power factor ($S^2\sigma_\tau$) (c) electrical conductivity (σ_τ) (d) thermal conductivity (k_{el}) of M_2PbC with temperature

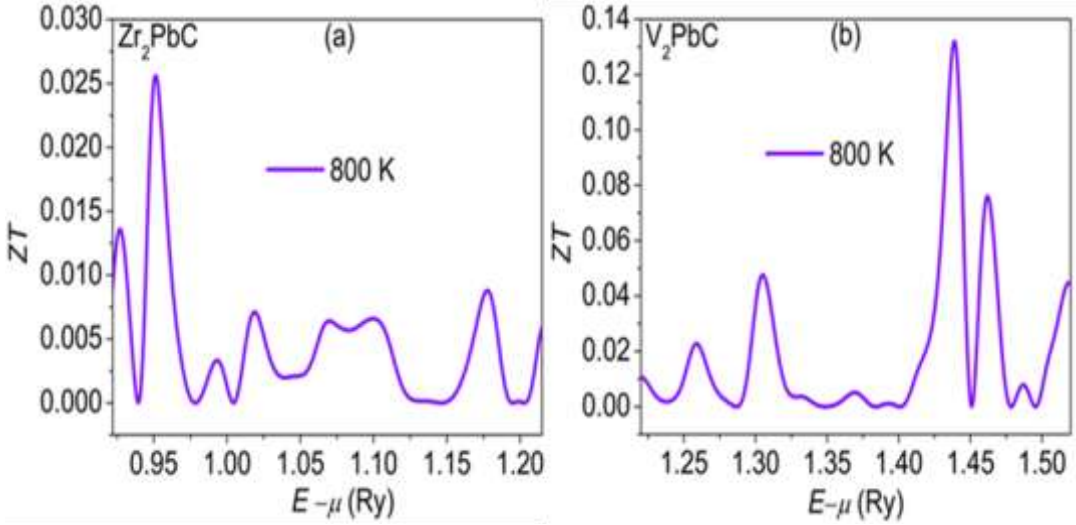

Figure 8. Energy dependence of ZT for (a) Zr_2PbC and (b)V_2PbC at 800 K

The relationship between the efficiency of thermoelectric power generation and the average ZT at 800 K showsthat V_2PbC is a more promising TE material than the bulk Zr_2PbC.

IV. CONCLUSIONS

We have studied the electronic and thermoelectric properties of Zr_2PbC, and V_2PbC using first-principles density functional theory, density functional perturbation theory, and Boltzmann transport theory, respectively. The electronic bands and TDOS show that both ternary MAX phases are metals with V_2PbC having the highest DOS at the E_F. The calculated Seebeck coefficients and ZT show that V_2PbC is a likely thermoelectric material in extreme conditions than Zr_2PbC and future thermoelectric material. Due to their relatively high electrical conductivities, these materials are potentially high-temperature conductive components manufacturing bye-products. It is hoped that further studies will help in the discovery of more new MAX phases that can replace the dominance of semiconducting devices as potential thermoelectric materials used in engineering technology.

V. ACKNOWLEDGMENT

The authors wish to thank MOHE Malaysia Grant: R.J13000.7854.5F231. ADSU, Mubi, Nigeria and TETFund, Nigeria. And acknowledge Dr. Yap Yung Szen, of the Physics Department, Universiti Teknologi Malaysia, for his technical advice and suggestions.

REFERENCES

[1] A. Berche and P. Jund, "Fully Ab-initio determination of the thermoelectric properties of half-Heusler NiTiSn: Crucial role of interstitial Ni defects," Materials (Basel)., vol. 11, no. 6, 2018, doi: 10.3390/ma11060868.

[2] M. Wolf, R. Hinterding, and A. Feldhoff, "High power factor vs. high zT-A review of thermoelectric materials for high-temperature application," Entropy, vol. 21, no. 11, 2019, doi: 10.3390/e21111058.

[3] T. Zhang et al., "Structure and Improved Thermoelectric Properties of Ag2 xCr2-2 xSe3 Compounds," Inorg. Chem., vol. 57, no. 19, pp. 12125–12131, 2018, doi: 10.1021/acs.inorgchem.8b01704.

[4] X. Zhang and L. Zhao, "Thermoelectric materials: Energy conversion between heat and electricity," J. Mater., vol. 1, no. 2, pp. 92–105, Jun. 2015, doi: 10.1016/j.jmat.2015.01.001.

[5] S. A. Khandy and J.-D. Chai, "Thermoelectric properties, phonon, and mechanical stability of new half-metallic quaternary Heusler alloys: FeRhCrZ (Z = Si and Ge)," J. Appl. Phys., vol. 127, no. 16, p. 165102, 2020, doi: 10.1063/1.5139072.

[6] Z. Kerrami, A. Sibari, O. Mounkachi, A. Benyoussef, and M. Benaissa, "Computational Condensed Matter SnO 2 improved thermoelectric properties under compressive strain," Comput. Condens. Matter, vol. 16, p. e00356, 2018, doi: 10.1016/j.cocom.2018.e00356.

[7] S. Ahmad, R. Ahmad, M. Bilal, and N. U. Rehman, "DFT studies of thermoelectric properties of R–Au intermetallics at 300 K,"

J. Rare Earths, vol. 36, no. 2, pp. 197–202, 2018, doi: 10.1016/j.jre.2017.08.004.

[8] U. Lachish, "Thermoelectric Effect Peltier Seebeck and Thomson," Guma Sci., no. 3, pp. 1–11, 2014, doi: 10.13140/EG.2.1.2722.3443.

[9] K. Hippalgaonkar et al., "High thermoelectric power factor in two-dimensional crystals of Mo S2," Phys. Rev. B, vol. 95, no. 11, 2017, doi: 10.1103/PhysRevB.95.115407.

[10] A. Gaul, Q. Peng, D. J. Singh, T. Borca-Tasciuc, and G. Ramanath, "Divalent doping-induced thermoelectric power factor increase in p-type Bi2Te3 via electronic structure tuning," J. Appl. Phys., vol. 125, no. 16, 2019, doi: 10.1063/1.5081438.

[11] A. Jayaraman, A. Bhat Kademane, and M. Molli, "DFT Study on the Carrier Concentration and Temperature-Dependent Thermoelectric Properties of Antimony Selenide," Indian J. Mater. Sci., vol. 2016, pp. 1–7, 2016, doi: 10.1155/2016/7296847.

[12] C. Wang, Y. Wang, G. Zhang, C. Peng, and G. Yang, "Theoretical investigation of the effects of doping on the electronic structure and thermoelectric properties of ZnO nanowires," Phys. Chem. Chem. Phys., vol. 16, no. 8, pp. 3771–3776, 2014, doi: 10.1039/c3cp54289k.

[13] J. R. Sootsman, D. Y. Chung, and M. G. Kanatzidis, "New and old concepts in thermoelectric materials," Angew. Chemie - Int. Ed., vol. 48, no. 46, pp. 8616–8639, 2009, doi: 10.1002/anie.200900598.

[14] M. Magnuson, M. Mattesini, N. Van Nong, P. Eklund, and L. Hultman, "Electronic-structure origin of the anisotropic thermopower of nanolaminated Ti 3SiC 2 determined by polarized x-ray spectroscopy and Seebeck measurements," Phys. Rev. B - Condens. Matter Mater. Phys., vol. 85, no. 19, pp. 1–8, 2012, doi: 10.1103/PhysRevB.85.195134.

[15] M. Khazaei et al., "Novel Electronic and Magnetic Properties of Two-Dimensional Transition Metal Carbides and Nitrides," pp. 2185–2192, 2013, doi: 10.1002/adfm.201202502.

[16] M. Khazaei, M. Arai, T. Sasaki, M. Estili, and Y. Sakka, "Two-dimensional molybdenum carbides: Potential thermoelectric materials of the MXene family," Phys. Chem. Chem. Phys., vol. 16, no. 17, pp. 7841–7849, 2014, doi: 10.1039/c4cp00467a.

[17] M. S. Ali, M. A. Rayhan, M. A. Ali, R. Parvin, and A. K. M. A. Islam, "New MAX Phase Compound Mo_2TiAlC_2: First-principles Study," J. Sci. Res., 2016, doi: 10.3329/jsr.v8i2.25057.

[18] A. Candan, S. Akbudak, Ş. Uğur, and G. Uğur, "Theoretical research on structural, electronic, mechanical, lattice dynamical and thermodynamic properties of layered ternary nitrides Ti2AN (A = Si, Ge and Sn)," J. Alloys Compd., vol. 771, no. August, pp. 664–673, Jan. 2019, doi: 10.1016/j.jallcom.2018.08.286.

[19] P. A. Burr, D. Horlait, and W. E. Lee, "Experimental and DFT investigation of (Cr,Ti)3AlC2MAX phases stability," Mater. Res. Lett., vol. 5, no. 3, pp. 144–157, 2017, doi: 10.1080/21663831.2016.1222598.

[20] A. Bouhemadou, "Structural, electronic and elastic properties of Ti_2TlC, Zr_2TlC and Hf_2TlC," Open Phys., vol. 7, no. 4, pp. 753–761, Jan. 2009, doi: 10.2478/s11534-009-0022-z.

[21] X. He, Y. Bai, Y. Li, C. Zhu, and M. Li, "Ab initio calculations for properties of MAX phases Ti_2InC, Zr_2InC, and Hf_2InC," Solid State Commun., vol. 149, no. 13–14, pp. 564–566, Apr. 2009, doi: 10.1016/j.ssc.2008.12.047.

[22] W. Luo and R. Ahuja, "Magnetic Fen+1ACn (n = 1, 2, 3, and A = Al, Si, Ge) phases: From ab initio theory," J. Phys. Condens. Matter, vol. 20, no. 6, pp. 2–5, 2008, doi: 10.1088/0953-8984/20/6/064217.

[23] H. Yang, B. Manoun, R. T. Downs, A. Ganguly, and M. W. Barsoum, "Crystal chemistry of layered carbide, $Ti_3(Si_{0.43}Ge_{0.57})C_2$ Hexiong," J. Phys. Chem. Solids, vol. 67, no. 12, pp. 2512–2516, 2006, doi: 10.1016/j.jpcs.2006.07.009.

[24] Y. Mo, P. Rulis, and W. Y. Ching, "Electronic structure and optical conductivities of 20 MAX-phase compounds," Phys. Rev. B - Condens. Matter Mater. Phys., vol. 86, no. 16, pp. 1–10, 2012, doi: 10.1103/PhysRevB.86.165122.

[25] D. J. Tallman et al., "A Critical Review of the Oxidation of Ti 2 AlC , Ti 3 AlC 2 and Cr 2 AlC in Air A Critical Review of the Oxidation of Ti 2 AlC , Ti 3 AlC 2 and Cr 2 AlC in Air," vol. 3831, 2013, doi: 10.1080/21663831.2013.806364.

[26] J. Nie, S. Liu, X. Zhan, L. Ao, and L. Li, "First-principles study of Hf/Nb/Zr-doped MAX phases Ti3AlC2 and Ti3SiC2," Phys.

B Condens. Matter, vol. 571, no. June, pp. 105–111, 2019, doi: 10.1016/j.physb.2019.06.052.

[27] A. Bouhemadou, "Calculated structural , electronic and elastic properties of M 2 GeC (M = Ti , V , Cr , Zr , Nb , Mo , Hf , Ta and W)," pp. 959–967, 2009, doi: 10.1007/s00339-009-5106-5.

[28] M. Atikur Rahman, "Study on Structural, Electronic, Optical and Mechanical Properties of MAX Phase Compounds and Applications Review Article," Am. J. Mod. Phys., vol. 4, no. 2, p. 75, 2015, doi: 10.11648/j.ajmp.20150402.15.

[29] Z. M. Sun, "Progress in research and development on MAX phases: a family of layered ternary compounds," Int. Mater. Rev., vol. 56, no. 3, pp. 143–166, 2011, doi: 10.1179/1743280410Y.0000000001.

[30] M. Naveed, A. F. Renteria, D. Nebel, and S. Weiß, "Study of high velocity solid particle erosion behaviour of Ti2AlC MAX phase coatings," Wear, vol. 342–343, pp. 391–397, 2015, doi: 10.1016/j.wear.2015.09.014.

[31] C. Xu et al., "An experimental and theoretical study of the hydrogen resistance of Ti_3SiC_2 and Ti_3AlC_2," Corros. Sci., vol. 142, no. December 2016, pp. 295–304, 2018, doi: 10.1016/j.corsci.2018.07.029.

[32] A. Heinzel, A. Weisenburger, and G. Müller, "Long-term corrosion tests of Ti_3SiC_2 and Ti2AlC in oxygen containing LBE at temperatures up to 700 °C," J. Nucl. Mater., vol. 482, pp. 114–123, Dec. 2016, doi: 10.1016/j.jnucmat.2016.10.007.

[33] C. Chen, F. Z. Li, C. H. Xu, H. B. Zhang, S. M. Peng, and G. J. Zhang, "High-temperature hydrogenation behaviour of bulk titanium silicon carbide," Adv. Appl. Ceram., vol. 115, no. 5, pp. 288–293, 2016, doi: 10.1080/17436753.2016.1144396.

[34] X. H. Wang and Y. C. Zhou, "• Invited Review Layered Machinable and Electrically Conductive Ti 2 AlC and Ti 3 AlC 2 Ceramics : a Review," J. Mater. Sci. Technol., vol. 26, no. 5, pp. 385–416, 2010, doi: 10.1016/S1005-0302(10)60064-3.

[35] J. Wang, X. Luo, and Y. Sun, "Torsional Fretting Wear Properties of Thermal Oxidation-Treated Ti3SiC2 Coatings," Coatings, vol. 8, no. 9, p. 324, Sep. 2018, doi: 10.3390/coatings8090324.

[36] M. F. Cover, O. Warschkow, M. M. M. Bilek, and D. R. McKenzie, "A comprehensive survey of M<sub>2</su>AX phase elastic properties," J. Phys. Condens. Matter, vol. 21, no. 30, 2009, doi: 10.1088/0953-8984/21/30/305403.

[37] E. N. Hoffman, D. W. Vinson, R. L. Sindelar, D. J. Tallman, G. Kohse, and M. W. Barsoum, "MAX phase carbides and nitrides : Properties for future nuclear power plant in-core applications and neutron transmutation analysis," Nucl. Eng. Des., vol. 244, pp. 17–24, 2012, doi: 10.1016/j.nucengdes.2011.12.009.

[38] X. K. Qian, H. Y. Wu, H. P. Zhu, S. H. Ma, and T. Jiang, "First-principles study of a new higher-order max phase of $Ti_5Al_2C_3$," J. Ceram. Sci. Technol., vol. 7, no. 1, pp. 47–52, 2016, doi: 10.4416/JCST2015-00027.

[39] I. V. Korobeinikov, L. N. Luk'yanova, G. V. Vorontsov, V. V. Shchennikov, and V. A. Kutasov, "Thermoelectric properties of n-Bi2Te3 - x - ySexSy solid solutions under high pressure," Phys. Solid State, vol. 56, no. 2, pp. 263–269, 2014, doi: 10.1134/S1063783414020152.

[40] K. Goc et al., "Structure, morphology and electrical transport properties of the Ti3AlC2 materials," Ceram. Int., vol. 44, no. 15, pp. 18322–18328, 2018, doi: 10.1016/j.ceramint.2018.07.045.

[41] D. Horlait, S. C. Middleburgh, A. Chroneos, and W. E. Lee, "Synthesis and DFT investigation of new bismuth-containing MAX phases," Scientific Reports, vol. 6. 2016. doi: 10.1038/srep18829.

[42] T. El-Raghy, S. Chakraborty, and M. . Barsoum, "Synthesis and characterization of Hf2PbC, Zr2PbC and M2SnC (M=Ti, Hf, Nb or Zr)," J. Eur. Ceram. Soc., vol. 20, no. 14–15, pp. 2619–2625, Dec. 2000, doi: 10.1016/S0955-2219(00)00127-8.

[43] S. J. Clark et al., "First principles methods using CASTEP," Zeitschrift für Krist. - Cryst. Mater., vol. 220, no. 5/6, pp. 567–570, Jan. 2005, doi: 10.1524/zkri.220.5.567.65075.

[44] M. A. Hadi, M. A. Rayhan, S. H. Naqib, A. Chroneos, and A. K. M. A. M. A. Islam, "Structural, elastic, thermal and lattice dynamic properties of new 321 MAX phases," Comput. Mater. Sci., vol. 170, no. May, p. 109144, 2019, doi: 10.1016/j.commatsci.2019.109144.

[45] P. Giannozzi et al., "QUANTUM ESPRESSO: a modular and open-source software project for quantum simulations of materials," J. Phys. Condens. Matter, vol. 21, no. 39, p. 395502, Sep. 2009, doi: 10.1088/0953-8984/21/39/395502.

[46] P. Giannozzi et al., "Advanced capabilities for materials modelling with Q UANTUM ESPRESSO," vol. 29, 2017, doi: 10.1088/1361-648X/aa8f79.

[47] G. K. H. Madsen, "BoltzTraP2, a program for interpolating band structures and calculating semi- classical transport coefficients," no. December 2017, 2018, doi: 10.1016/j.cpc.2018.05.010.

[48] G. K. H. Madsen and D. J. Singh, "BoltzTraP. A code for calculating band-structure dependent quantities," Comput. Phys. Commun., vol. 175, no. 1, pp. 67–71, 2006, doi: 10.1016/j.cpc.2006.03.007.

[49] J. P. Perdew, K. Burke, and M. Ernzerhof, "Generalized Gradient Approximation Made Simple," Phys. Rev. Lett., vol. 77, no. 18, pp. 3865–3868, Oct. 1996, doi: 10.1103/PhysRevLett.77.3865.

[50] H. J. Monkhorst and J. D. Pack, "Special points for Brillonin-zone integrations* Hendrik," Phys. Rev. B, vol. 13, no. 12, pp. 5188–5192, 1976, doi: 10.1103/physrevb.13.5188.

[51] G. K. H. Madsen, J. Carrete, and M. J. Verstraete, "BoltzTraP2, a program for interpolating band structures and calculating semi-classical transport coefficients," Comput. Phys. Commun., vol. 231, pp. 140–145, 2018, doi: 10.1016/j.cpc.2018.05.010.

[52] K. Capelle, "A bird's-eye view of density-functional theory," Brazilian J. Phys., vol. 36, no. 4a, pp. 1318–1343, Dec. 2006, doi: 10.1590/S0103-97332006000700035.

[53] M. B. Kanoun, S. Goumri-Said, A. H. Reshak, and A. E. Merad, "Electro-structural correlations, elastic and optical properties among the nanolaminated ternary carbides Zr_2AC," Solid State Sci., vol. 12, no. 5, pp. 887–898, 2010, doi: 10.1016/j.solidstatesciences.2010.01.035.